Langmuir

Article

pubs.acs.org/Langmuir

Electrocatalytic Amplification of Single Nanoparticle Collisions Using DNA-Modified Surfaces

Timothy M. Alligrant, Radhika Dasari, Keith J. Stevenson, and Richard M. Crooks*

Department of Chemistry and Center for Nano- and Molecular Science and Technology, The University of Texas at Austin, 105 E. 24th St., Stop A5300, Austin, Texas 78712-0165 United States

Supporting Information

ABSTRACT: Here we report on the effect of DNA modification on individual collisions between Pt nanoparticles (PtNPs) and ultramicroelectrode (UME) surfaces. These results extend recent reports of electrocatalytic amplification (ECA) arising from collisions between naked surfaces, and they are motivated by our interest in using ECA for low-level biosensing applications. In the present case, we studied collisions between naked PtNPs and DNA-modified Au and Hg UMEs and also collisions between DNA-modified PtNPs and naked Au and Hg UMEs. In all cases, the sensing reaction is the catalytic oxidation of N_2H_4. The presence of ssDNA (5-mer or 25-mer) immobilized on the UME surface has little effect on the magnitude or frequency of ECA signals, regardless of whether the electrode is Au or Hg. In contrast, when DNA is immobilized on the PtNPs and the electrodes are naked, clear trends emerge. Specifically, as the surface concentration of ssDNA on the PtNP surface increases, the magnitude and frequency of the current transients decrease. This trend is most apparent for the longer 25-mer. We interpret these results as follows. When ssDNA is immobilized at high concentration on the PtNPs, the surface sites on the NP required for electrocatalytic N_2H_4 oxidation are blocked. This leads to lower and fewer ECA signals. In contrast, naked PtNPs are able to transfer electrons to UMEs having sparse coatings of ssDNA.

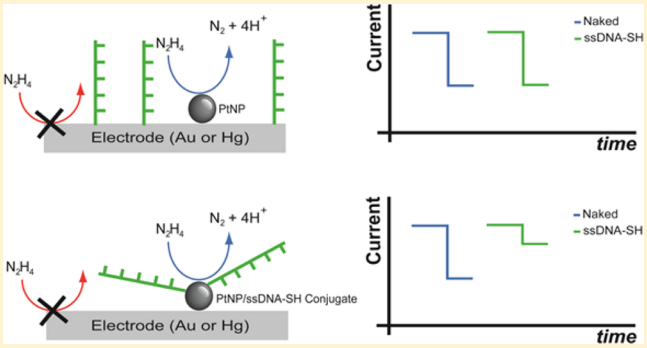

INTRODUCTION

When an electrochemical cell is configured with a redox molecule that exhibits sluggish electron-transfer kinetics at an electrode, little current is observed. If catalytically active nanoparticles (NPs) are present in solution and the electrode is appropriately poised, however, current transients are observed when they collide with the electrode. This phenomenon is known as electrocatalytic amplification (ECA).[1−3] We are interested in using the principles of ECA to develop single-molecule electrochemical sensors, and toward that end we report here on how single-strand DNA (ssDNA), immobilized on either the electrode or the NP, affects the ECA current−time (i−t) response. Specifically, as shown in Scheme 1, we compare the current signatures of collisions of naked and ssDNA-modified PtNPs with naked and ssDNA-modified Au and Hg ultramicroelectrodes (UMEs). Two key findings emerge from this study. First, the presence of ssDNA monolayers immobilized on UMEs (Scheme 1a) have little impact on the frequency or magnitude of current transients arising from collisions with naked PtNPs. Second, if the PtNPs are modified with ssDNA but the electrode remains naked (Scheme 1b), then a significant influence is observed in both the collision frequency and current transient magnitude.

ECA, originally reported by Bard and co-workers,[1] is carried out by poising an electrode (Au,[4] Pt,[5] PtOx,[6] carbon,[4] boron-doped diamond,[7] Hg,[8] or Bi[9]) at a potential where little faradaic current flows in the presence of an electroactive redox-probe molecule (N_2H_4, H_2O, H_2O_2, H^+, O_2, or BH_4^-).[1,7−10] Upon addition of NPs (Au,[6] Pt,[4,11] or IrO_x[5]), which are catalytic for the reduction or oxidation of the redox probe molecule, current transients are observed. Each of these transients arises from a collision between a catalytic particle and the noncatalytic working electrode. In addition to the Bard group, the Alpuche-Aviles,[12] Andreescu,[13] Compton,[14−17] Crooks,[18−21] Koper,[22,23] Macpherson,[7] Stevenson,[8−10] Unwin,[22] Yang,[24] and Zhang[25−28] groups have all contributed significantly to our understanding of ECA.

The results reported here build specifically upon prior reports from the Bard,[11,29] Stevenson,[8] and Crooks[18] groups. For example, the Bard group examined how carboxylic-acid-terminated n-alkanethiol monolayers on either the electrode surface or on the PtNPs affect ECA current transients.[29] They discovered that as the length of the n-alkanoic acid increased from 3 to 16 carbons, the collision frequency and the size of the current transients decreased, regardless of whether the monolayer was immobilized on the UME or the PtNPs.

Received: July 15, 2015
Revised: August 26, 2015
Published: October 12, 2015

   DOI: 10.1021/acs.langmuir.5b02620

Scheme 1[a]

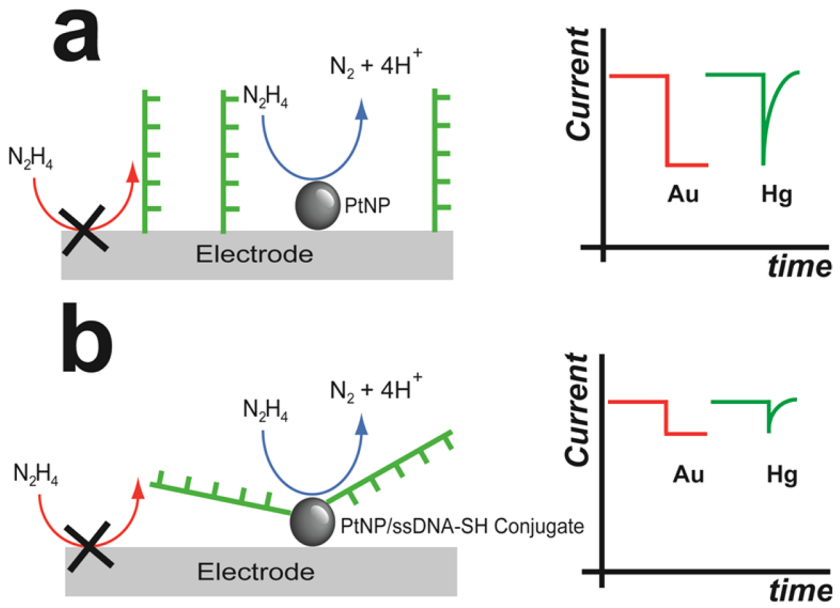

[a](a) The magnitude and frequency of collision transients are unaffected when the electrode surface is modified with ssDNA. (b) Modification of the nanoparticle with ssDNA decreases the magnitude and frequency of colliding nanoparticles.

Additionally, higher coverages of *n*-alkanoic acids led to lower collision frequencies and lower current magnitudes.

Our group utilized the ECA technique to detect individual DNA hybridization events using a microelectrochemical flow system.[18] In this case, a Au electrode within the device was modified with ssDNA and poised at a potential where N_2H_4 was not readily oxidized. The microelectrochemical cell was then filled with an electrolyte solution containing N_2H_4, and a small residual background current due to N_2H_4 oxidation was observed. However, when ssDNA/PtNP conjugates were admitted to the flow channel, larger current transients, corresponding to individual DNA hybridization events, were observed. In the present work, we are not concerned with hybridization per se, rather, as a precursor to forthcoming sensor studies, the focus here is on developing a fundamental understanding of the effect of immobilized ssDNA on the collision frequency and current transient magnitude using N_2H_4 as the redox probe.

One of the fundamental problems with ECA experiments relates to the background current, which in turn defines the minimum current transient size (i.e., smallest detectable S/N ratio) that can be quantitatively measured. This response is a particularly important point for sensing applications of ECA, where NP labels are likely to be small (a few nanometers), which results in small collision currents relative to the background. As alluded to earlier, a second problem with using ECA for sensing applications is that the current transients are long-lived and step-shaped, and the background current increases with time as a result of NP accumulation. To address these points, one of us (Stevenson and co-workers)[8−10] discovered that the use of Hg electrodes suppresses the background current by 2 orders of magnitude compared to Au UMEs and gives rise to short-lived current transients that are spike-shaped and that decay to the background current level (Scheme 1).

In the current ECA study, we systematically and quantitatively evaluated both ssDNA-modified and naked Hg and Au UMEs for the electrocatalytic oxidation of N_2H_4 using both naked and ssDNA-modified PtNPs. Two different length ssDNA oligomers were examined: a 5-mer and a 25-mer (Table 1). The results show that modification of the electrode surface with ssDNA has little effect on the collision frequency or transient size on either the Hg or Au UMEs, regardless of the length of the ssDNA or its coverage. However, modification of the PtNPs with six different ssDNA-to-PtNP ratios (5:1 to 50:1) results in a significant change in both the frequency and the transient size even though the ssDNA coverage is low (just 2−7 ssDNA strands per NP). For example, compared to naked PtNPs, average decreases of ∼9% and 70% are observed for the 5-mer and 25-mer, respectively, and the transient size decreases an average of ∼86%.

Table 1. Surface Modifiers Used in This Study with Accompanying Physical Data

name	sequence	number of bases	length (nm)[a]
MPOH	HO-$(CH_2)_3$-SH	0	0.52
5-mer	5′-GCG CG-$(CH_2)_3$-SH-3′	5	2.6
25-mer	5′-CAC GAC GTT GTA AAA CGA CGG CCA G-$(CH_2)_3$-SH-3′	25	10.4

[a]Determined from optimized geometry in ArgusLab,[45] (MPOH) and known standard distance between nucleotides in ssDNA (0.34 nm).[46]

EXPERIMENTAL SECTION

Chemicals and Materials. The following chemicals were purchased from Sigma-Aldrich (St. Louis, MO) and used as received: $N_2H_4{\cdot}H_2O$ (64% N_2H_4, 98%), $H_2PtCl_6{\cdot}(H_2O)_6$ (99.9%), tris(hydroxymethyl)-aminomethane (tris-HCl, 99.8%), and $Hg_2(NO_3)_2$ (98.0%). The following chemicals were purchased from Fisher Scientific (Fair Lawn, NJ) and used as received: tris(2-carboxyethyl)phosphine hydrochloride (TCEP, 98%), hexaammineruthenium(III) chloride ($Ru(NH_3)_6^{3+}$, 98%), $NaH_2PO_4{\cdot}(H_2O)_2$ (100%), KNO_3 (100%), NaCl (100%), and HNO_3 (69.3% in water). The following additional chemicals were used as received: $NaBH_4$ (98.0%, Acros Organics), sodium citrate (99.0%, Alfa Aesar), NaOH (97.0%, EMD Chemical), ethanol (99.5%, anhydrous, Pharmco-AAPER, Brookfield, CT), and mercaptopropanol (MPOH,

97+%, Acros Organics). Deionized water (DI H_2O) from a Millipore filtration system (Milli-Q gradient system, Millipore, Bedford, MA) having a resistivity of 18.2 MΩ·cm was used for all experiments. All ssDNA oligonucleotides (sequences in Table 1) were synthesized and purified (high-performance liquid chromatography) by Integrated DNA Technologies (Coralville, IA) and received as lyophilized pellets. Once received, the lyophilized pellets were rehydrated in a solution containing 10 mM tris-HCl and 150 mM NaCl (pH 7.4).

PtNP Synthesis and Modification with ssDNA. PtNPs were synthesized using a previously reported procedure.[8−10,30] First, 7.76 mL of 0.20% (w/v) H_2PtCl_6 was added to 100 mL of boiling DI water. Second, this solution was allowed to boil for ∼1 min before adding 2.37 mL of a solution containing 1% (w/v) sodium citrate and 0.05% (w/v) citric acid. Third, the solution was allowed to boil for an additional ∼30 s prior to addition of 1.18 mL of a freshly prepared solution containing 0.08% (w/v) $NaBH_4$, 1% (w/v) sodium citrate, and 0.05% (w/v) citric acid. The solution was then allowed to boil for an additional 10 min. Upon addition of the $NaBH_4$ solution the color of the H_2PtCl_6/citrate mixture became dark, indicating formation of PtNPs. Next, the product was cooled to 24−25 °C and then dialyzed for 24 h to remove excess salts.

Transmission electron microscopy (TEM, FEI Tecnai G^2 Spirit) was used to determine the size of the PtNPs (4.2 ± 0.9 nm, Figure S1). The PtNP concentration was determined by dividing the concentration of H_2PtCl_6 by the number of Pt atoms[31] contained within a spherical 4.2 nm particle.[11] The concentration calculations are based on the assumption that H_2PtCl_6 is completely reduced to zerovalent Pt.

Preparation of the ssDNA-modified PtNP conjugates followed previously described methods.[18,32−34] Briefly, the ssDNA/PtNP conjugates were prepared by mixing 1.2 mM disulfide ssDNA with 120 mM TCEP in a 1:1 ratio for 1 h in the dark at 24−25 °C to reduce the disulfide. Once reduced, 900 μL of the stock PtNP solution (120 nM) was added to the ssDNA-SH/TCEP solution, followed by sufficient 1.0 M phosphate buffer (pH 7.0) to bring the total volume to 1.0 mL. This solution was allowed to stand in the dark for 24 h at 24−25 °C. The MPOH/PtNP conjugates were prepared using similar conditions.

Electrode Preparation. The preparation, cleaning, and electrochemical characterization of UMEs, including Hg electrodeposition, has been reported previously, and details are provided in the Supporting Information (Figure S2).[11,29,35,36]

Modification of both Hg and Au UMEs with ssDNA was performed at open-circuit potential (OCP) in solutions containing ssDNA, 10 mM tris-HCl buffer, and 0.15 M NaCl (pH 7.4). Hg UMEs were modified with two different ssDNA concentrations (1.0 and 4.0 μM) for time periods of either 5 or 60 s. The Au UMEs were modified using 10.0 μM ssDNA for 2 h. Different modification conditions were used for the Hg and Au UMEs because high ssDNA surface coverages (∼10^{13} ssDNA cm^{-2}) are easier to achieve on Hg relative to Au.[37−39] Au macroelectrodes (3.0 mm, CH Instruments, Austin, TX) were modified using conditions similar to those used to modify the Au UMEs.

Electrochemical Experiments. Cyclic voltammetry (CV) and current−time (i−t) curves obtained using Hg and Au UMEs were measured using instrumentation described previously.[18] A ChemClamp voltammeter-amperometer (Dagan Corp., Minneapolis, MN) served as the potentiostat, while the voltage signal was generated by a PAR 175 Universal Function Generator (Princeton Applied Research, Oak Ridge, TN). This setup was interfaced to a Dell Optiplex 380 computer through a PCI-6251 data acquisition board (National Instruments, Austin, TX) via a BNC-2090A analog breakout accessory (National Instruments). Two-electrode cell connections from a preamplifier were housed in a Faraday cage constructed using copper plate and mesh. The CV data and i−t curves were measured using custom software written in LabView 2010 (National Instruments). The sampling time for measuring CVs and i−t curves was 15 ms.

Electrochemical cleaning of the Pt and Au UMEs, Hg electrodeposition, and square-wave voltammetry (SWV) were performed using a CHI 650C potentiostat (CH Instruments). All three-electrode electrochemical experiments (those performed using the CHI 650C potentiostat) utilized a Pt wire counter electrode (CH Instruments) and a "leakless" Ag/AgCl (3.4 M KCl) reference electrode (model 66-EE009, Dionex, Bannockburn, IL). This same "leakless" Ag/AgCl reference was used for the two-electrode configuration mentioned above. The total volume of all electrochemical solutions was 25.0 mL, and each was degassed with N_2 for at least 30 min prior to data collection. The potential used for measuring i−t curves was adjusted so that the background current was in the range ∼ −0.05 to −0.10 nA.

RESULTS AND DISCUSSION

Collisions between Naked PtNPs and ssDNA-Modified Au UMEs. The experiments described in this section were carried out as follows. First, Au UMEs were modified with ssDNA. Second, background CVs and i−t curves (in the absence of PtNPs) were obtained in a solution containing 10.0 mM N_2H_4 and 50 mM phosphate buffer at pH 7.0 (hereafter referred to as N_2H_4/buffer solution). Third, collision experiments with naked PtNPs were carried out. Complete details of the procedure used to modify the Au UMEs with ssDNA are outlined in the Experimental Section and Supporting Information.

Surface concentrations of ssDNA were determined using Au macroelectrodes (3 mm diameter) modified using conditions equivalent to those used for the Au UMEs. The macroelectrodes were used as proxies for the UMEs, because the latter had insufficient surface area to provide accurate surface coverage data using the well-known Tarlov method.[40,41] Full details regarding surface coverage experiments and calculations are provided in the Supporting Information. The results indicated average coverages of the 5-mer and 25-mer were $(2.8 \pm 1) \times 10^{13}$ 5-mer/cm^2 and $(1.2 \pm 0.9) \times 10^{13}$ 25-mer/cm^2. This means that there is only ∼1% of a monolayer of ssDNA on the electrode surface, leaving numerous naked patches between oligomers. These spaces are sufficient to allow ∼4.2 nm PtNP to collide with the electrode.

Figure 1a shows CVs of a naked and a 5-mer-modified Au UME obtained using N_2H_4/buffer solution. These CVs serve two important purposes. First, they provide qualitative evidence that the electrode is modified with ssDNA. That is, the shift in the wave toward more positive potentials and the lowering of the mass-transfer-limited current after modification with ssDNA are characteristic of partially blocked electrodes.[29,42] These two effects are particularly pronounced for inner-sphere redox reactions, such as the N_2H_4 oxidation used in these experiments, because electron transfer requires intimate contact with the electrode surface.[42] Second, the onset potentials of these two CVs provide a basis for selecting the optimal potential for obtaining i−t collision data (*vide infra*). The onset potential is defined here as the potential at which the faradaic current increases beyond the nonfaradaic background current by −0.05 to −0.10 nA (anodic currents are designated as negative).

Prior to collision experiments, a background i−t response for the 5-mer-modified electrode was obtained in the same N_2H_4/buffer solution used to generate the red CV in Figure 1a. The potential of the UME was set to the onset potential, which is defined in the previous paragraph. Because this experiment was carried out in the absence of PtNPs, no current transients were observed (data not shown). Next, naked PtNPs were injected into the solution such that the final concentration was 10 pM, and an i−t trace was recorded at the same electrode potential used for the background scan. Figure 2a displays i−t traces recorded on naked (black) and 5-mer-modified (red) Au UMEs. Results for the same experiment, except using a 25-mer-modified Au UME, are provided in the Supporting Information (Figure S3). As shown in the expanded view (Figure 2b) both i−t curves exhibit the familiar step-shaped current transients previously

DOI: 10.1021/acs.langmuir.5b03639

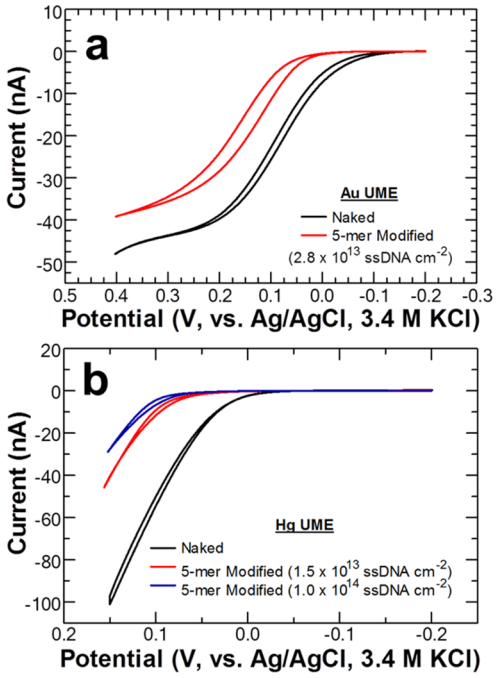

Figure 1. CVs of 10.0 mM N_2H_4 obtained using naked and 5-mer-modified UMEs. (a) CVs obtained using a naked Au UME (black trace) and a Au UME after modification with 5-mer ssDNA (red trace). (b) CVs obtained using a naked Hg UME (black trace) and Hg UMEs after ssDNA modification (red and blue traces). The 5-mer coverages are indicated in the legends. In all cases, the electrolyte contained 50.0 mM phosphate buffer (pH 7.0) and the scan rate was 20 mV/s.

reported by Bard and co-workers.[11] Another interesting and potentially important observation is that the background currents observed for the ssDNA-modified Au UMEs are much more stable for the duration of the collision experiments compared to the nominally naked Au UMEs (Figures 2a and S3).

The histograms in Figure 2c were extracted from the $i-t$ data in Figure 2a, and they show the number of collisions for each current amplitude detected at both naked (black bins) and 5-mer-modified Au UMEs (red bins). Using a previously reported model,[1] the expected magnitude of the collision current is ~64 pA (see the Supporting Information), while the distributions in Figure 2c have mean values of 39 ± 25 and 44 ± 31 pA for the naked and 5-mer-modified Au UMEs, respectively. The approach used for calculating the expected collision current is rather crude,[11] and together with the likelihood that some PtNPs are agglomerated (resulting in larger currents than single particles),[23] this level of agreement is quite reasonable. The distribution in Figure 2c has a t-test value of t = 1.05 (134 degrees of freedom, DOF) when evaluating the statistical variance between event populations of PtNP collisions at naked and 5-mer-modified Au UMEs. Therefore, we can state with 99.95% confidence (t = 3.37) that there is no significant difference in the detected current transients resulting from collisions between PtNPs and naked or 5-mer-modified Au UMEs. Moreover, only a slight decrease in current magnitude is observed when the length of the ssDNA is extended to a 25-mer (Table 2).

As shown Table 2, the average collision frequency for all experiments carried out using Au UMEs was 0.015 ± 0.005 pM^{-1} s^{-1}, regardless of whether the electrode was naked or modified with either of the ssDNA oligonucleotides (5-mer or 25-mer). In other words, the presence of the ssDNA monolayer also has a negligible effect on the collision frequency. Note that the tabulated collision frequencies are comparable in magnitude to previous results reported by Bard and co-workers (0.012−0.02 pM s^{-1}) for ~3.6 nm PtNPs.[11]

Collisions between Naked PtNPs and ssDNA-Modified Hg UMEs. With the following two exceptions, experiments involving collisions between naked PtNPs and naked or ssDNA-modified Hg UMEs were similar to those described for Au UMEs. First, modification of Hg UMEs with ssDNA required less time (5−60 s vs 2 h for Au) and lower ssDNA solution concentrations (1.0−4.0 μM vs 10.0 μM for Au). Second, the coverage of ssDNA on the Hg UMEs was determined using an electrochemical stripping method[38,43] rather than the Tarlov approach described earlier.

After modification of the Hg UMEs with the 5-mer ssDNA, CVs were obtained in N_2H_4/buffer solutions. Figure 1b shows three CVs: the black CV was obtained using a naked Hg UME, and the other two using independently prepared 5-mer-modified Hg UMEs. The Hg electrodes used for the red and blue CVs were modified with ssDNA for 5 s in 1.0 μM ssDNA and 60 s in 4.0 μM ssDNA, respectively. The DNA coverage on each Hg electrode, which corresponds to 1−10% of a monolayer, is provided in the legend of Figure 1b. Like the CVs measured on the naked and 5-mer modified Au UMEs (Figure 1a), the onset of faradaic current shifted from ~ −0.05 V on the naked electrode to ~0.05 V on the 5-mer modified Hg UMEs.

The aforementioned current onset potentials were used for the collision experiments. After setting the Hg electrode potential, 10 pM naked PtNPs were introduced into the solution, which resulted in spike-shaped current transients regardless of whether the Hg UME was naked or modified with 5-mer ssDNA (Figure 2d and expanded view in Figure 2e). A similar experiment was carried out for a Hg UME modified with 25-mer ssDNA (Figure S3). In all cases, the current transients at both the naked and ssDNA-modified Hg UMEs were found to be similar in magnitude and shape to those described by Stevenson and co-workers for collisions of PtNPs at naked Hg electrodes.[8,10]

The histogram in Figure 2f summarizes the collision data obtained from the $i-t$ traces in Figure 2d. Note that for collisions at Hg electrodes, it is conventional to report the magnitude of the collisions in terms of charge under the peak-shaped transient,[8] rather than the maximum current change as is the custom for solid electrodes. The experimentally measured mean charges for collisions at naked and 5-mer-modified Hg UMEs are 30 ± 21 and 35 ± 18 pC, respectively, while the expected magnitude of the charge is ~64 pC (see the Supporting Information). The histograms in Figure 2f have a t-test value of t = 2.06 (257 DOF) when evaluating the statistical variance between the two populations of PtNP collisions at naked and 5-mer modified Hg UMEs. Accordingly there is no significant difference between the two sets of collision data (99.95% certainty, t = 3.33). In other words, the presence of the 5-mer ssDNA on the Hg UME does not affect the charge due to N_2H_4 oxidation resulting from collisions. Data similar to these were also obtained for a 25-mer-modified Hg UME, and the results are provided in Table 2 and Figure S3.

Table 2 collects the collision frequencies and charges recorded for naked and ssDNA-modified Hg UMEs averaged over all experiments performed. Regardless of the presence or absence of ssDNA on the Hg UME, oligomer length, or surface coverage, the average collision frequency is 0.022 ± 0.007 pM^{-1} s^{-1}. This value is somewhat larger than that recorded on Au UMEs (0.015 ± 0.005 pM^{-1} s^{-1}) but very close to values reported by Stevenson

DOI: 10.1021/acs.langmuir.5b03639

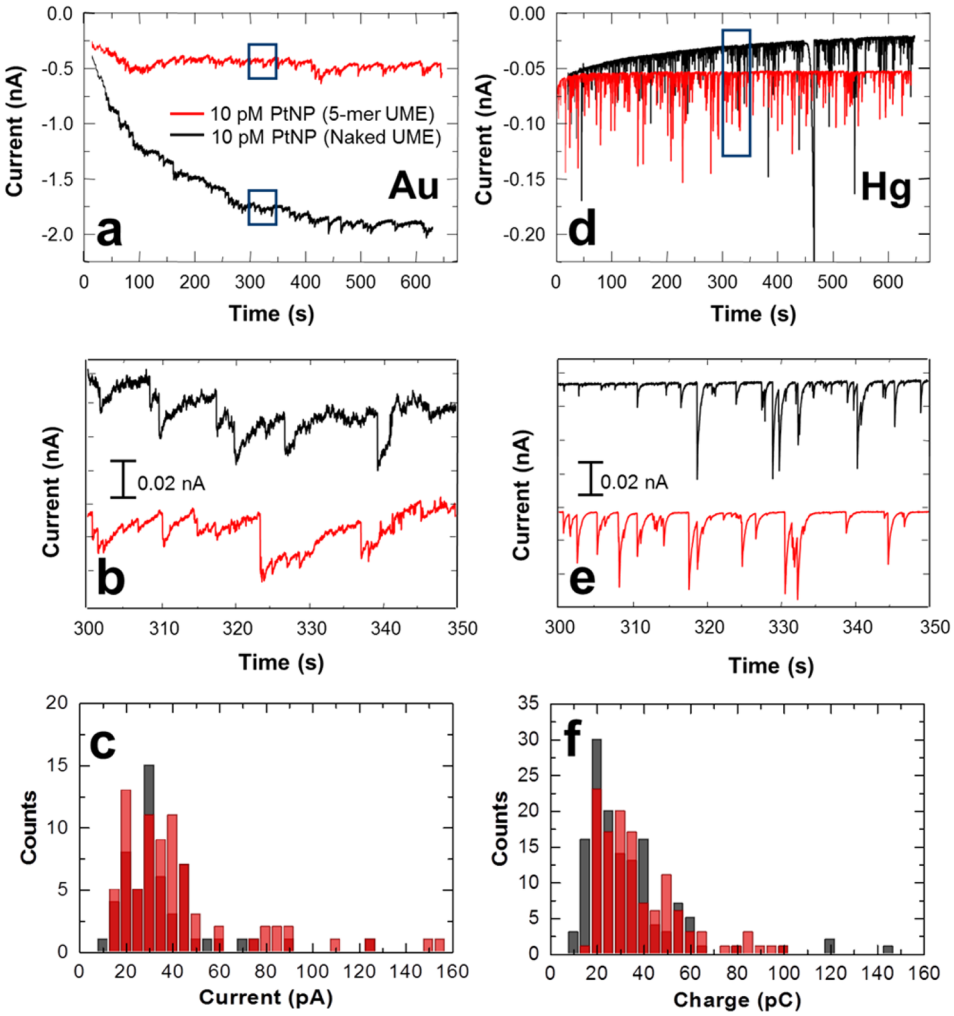

Figure 2. Chronoamperometric data and associated histograms for collisions between naked PtNPs and naked or ssDNA-modified Au and Hg UMEs. Results for naked (black) and 5-mer modified (red) (a–c) Au and (d-f) Hg UMEs. The data were obtained using N_2H_4/buffer solutions and 10 pM PtNPs. The 5-mer coverages on the Au and Hg UMEs were $(2.8 \pm 1) \times 10^{13}$ and 2.0×10^{13} 5-mer cm^{-2}, respectively. The legend in (a) applies to all plots. The black rectangles in (a) and (d) indicate the approximate location of the data displayed in (b) and (e), respectively. The histograms (c and f) exclude current transients larger than 200 pA, because they arise from agglomerated PtNPs.[23] The red bins in the histograms (c and f) are semitransparent and are in front of the black bins. This means the light pink color indicates where the population for the 5-mer-modified UME bin exceeds that of the naked UME bin behind it.

Table 2. Average Collision Frequencies and Transient Sizes Measured at Naked and Modified Hg and Au UMEs in the Presence of Naked 10 pM PtNPs (~4.2 nm)[a]

electrode	modification (conditions used)	frequency (pM^{-1} s^{-1})	transient size	coverage ($\times 10^{13}$ ssDNA cm^{-2})
Au	naked	0.011 ± 0.004	49 ± 24 pA	
	5-mer (2 h, 10.0 μM)	0.015 ± 0.001	50 ± 26 pA	2.8 ± 1
	25-mer (2 h, 10.0 μM)	0.018 ± 0.008	35 ± 22 pA	1.2 ± 0.9
	MPOH	0.014 ± 0.006	50 ± 25 pA	7.7 ± 5
Hg	naked	0.024 ± 0.006	40 ± 17 pC	
	5-mer (5 s, 1.0 μM)	0.024 ± 0.006	43 ± 20 pC	2.4 ± 0.7
	5-mer (60 s, 4.0 μM)	0.021 ± 0.008	47 ± 35 pC	10 ± 0.2
	25-mer (5 s, 1.0 μM)	0.020 ± 0.004	48 ± 30 pC	0.48 ± 0.05
	25-mer (60 s, 4.0 μM)	0.022 ± 0.006	56 ± 35 pC	4.9 ± 2
	MPOH	0.023 ± 0.007	41 ± 34 pC	10 ± 0.6

[a]The error represents the standard deviation from the mean for three independent experiments.

and co-workers (0.024 pM^{-1} s^{-1}) for collisions between ~4.7 nm PtNPs and naked Hg UMEs.[8] The average collision charges recorded for naked PtNPs colliding with both naked and ssDNA-modified Hg UMEs was 47 ± 27 pC. This value is similar to the expected charge of 64 pC calculated using somewhat tenuous assumptions (see the Supporting Information).

Collisions between Naked PtNPs and MPOH-Modified Au and Hg UMEs. As discussed earlier, ssDNA oligomers are

DOI: 10.1021/acs.langmuir.5b02630

received as disulfides (DNA-C_3-S-S-C_3-OH) and then chemically reduced prior to use. Therefore, one of the disulfide cleavage products is mercaptopropanol (MPOH), and hence both the Au and Hg electrodes (and, as discussed later, PtNPs) are exposed to both MPOH and ssDNA-SH simultaneously. Accordingly, we carried out control experiments by modifying electrodes with just MPOH (no ssDNA) to better understand its effect on collision-induced $i-t$ traces. Au and Hg UMEs were modified with MPOH using the same procedure as for ssDNA.

Figure S3 shows $i-t$ traces, obtained in N_2H_4/buffer solutions, before and after introduction of 10 pM naked PtNPs. The results reveal step- and spike-shaped current transients for Au[11] and Hg[8,10] UMEs, respectively. The collision frequencies are 0.014 ± 0.006 and 0.023 ± 0.007 pM^{-1} s^{-1} for the Au and Hg UMEs, respectively, and the magnitude of the transients are 50 ± 25 pA and 41 ± 34 pC, respectively. These metrics are similar to those determined using naked Au and Hg UMEs (Table 2): 0.011 ± 0.004 pM^{-1} s^{-1} and 49 ± 24 pA for Au and 0.024 ± 0.006 pM^{-1} s^{-1} and 40 ± 17 pC for Hg. They are also similar to values measured at ssDNA-modified UMEs and those previously reported by the Bard[11] and Stevenson[8] groups.

The surface coverage for MPOH on Au and Hg UMEs was determined via electrochemical stripping, as described in the Supporting Information, and found to be (7.7 ± 5) × 10^{13} and (10 ± 0.6) × 10^{13} MPOH/cm^2, respectively. This coverage is higher than for ssDNA on either of the UMEs, likely due to the shorter length of the molecule (Table 1) and its neutral charge. A significant difference between the collision frequency and transient size at naked and MPOH-modified UMEs would be unreasonable, as electrons should be able to tunnel through this SAM. For example, Bard and co-workers found virtually no change in the collision frequency or current amplitude for naked PtNPs colliding with 3-mercaptopropanoic acid-modified Au UMEs.[29] We conclude that the presence of MPOH on either Au or Hg UMEs does not exert a significant perturbation on collision signal frequencies and magnitudes by naked PtNPs.

Collisions between ssDNA- or MPOH-Modified PtNPs and Naked Au UMEs. In addition to studying collisions between naked PtNPs and modified electrode surfaces, we also examined the inverse case: ssDNA-modified PtNPs (ssDNA/PtNPs) colliding with nominally naked electrodes. These experiments were carried out as follows. First, the PtNPs were modified with one of the thiol derivitives (5-mer, 25-mer, or MPOH). Second, the naked UMEs were placed into the N_2H_4/buffer solution and background CVs and $i-t$ curves were measured in the absence of PtNPs. Third, 10 pM PtNPs (naked or modified) were introduced to the solution and an $i-t$ curve was measured for ~600 s.

For these experiments, six sets of ssDNA/PtNP conjugates were prepared using ssDNA:PtNP ratios ranging from 5:1 to 50:1. The ssDNA/PtNP conjugates were prepared using a method similar to that described in previous reports.[18,32−34] Note that the indicated ssDNA:PtNP ratios are those used for preparation of the ssDNA/PtNP conjugates, but the actual average coverages of ssDNA on the PtNPs are lower due to <100% adsorption and ssDNA desorption during washing steps. Washing is important, because it removes free ssDNA from solution and therefore minimizes contamination of the otherwise naked electrodes. Details regarding experimental determination of the actual average coverages of 25-mer ssDNA on the PtNPs is provided in the Supporting Information. The measured 25-mer coverages ranged from 6.9 × 10^{11} to 23 × 10^{11} ssDNA/cm^2, or from 2.1 (for the 5:1 solution ratio) to 7.0 (for the 50:1 solution ratio) oligonucleotides per PtNP (Table S1).

After collecting a background CV (black trace in Figure 1a) and background $i-t$ curve in N_2H_4/buffer solution alone (not shown), 10 pM PtNPs were introduced to the solution. Figure 3a presents seven $i-t$ curves measured in the presence of naked PtNPs and at each of the 5-mer ssDNA:PtNP ratios. Equivalent $i-t$ plots, for PtNPs modified with either 25-mer ssDNA or MPOH are provided in Figures S4 and S5. As is typical for Au electrodes, all of the $i-t$ transients exhibit step-shaped collision features.[1,11,29]

Figure 3a−d shows that as the 5-mer ssDNA:PtNP ratio increases, the magnitude of current due to PtNP collisions decreases. For example, the average collision amplitude for naked PtNPs colliding with a naked Au UME is 49 ± 24 pA (Figure 3b), but for PtNPs modified with a 5:1 5-mer ssDNA:PtNP ratio, the collision amplitude decreases to 28 ± 13 pA (Figure 3c).

Additional insight into the effect of PtNP functionalization is provided by the results shown in Figure 3e and f. These plots display the collision frequency and amplitude, respectively, as a function of the 5-mer:PtNP solution ratio used to prepare the 5-mer/PtNP conjugates (lower horizontal axis) and the actual 25-mer ssDNA surface coverage (upper horizontal axis). Due to the short length of the 5-mer, it was not possible to measure its actual surface coverage. The collision frequencies for both the 5-mer- and 25-mer-modified PtNPs are hardly distinguishable from naked PtNPs (open circle, 0.011 ± 0.004 pM^{-1} s^{-1}), but there is a trend suggesting lower collision frequencies for the 25-mer-modified PtNPs. This is especially apparent at the highest surface coverages, and hence it might be due to the slightly lower diffusion coefficient of PtNPs that are modified with the longer ssDNA.

Though only a small change in the collision frequency is observed over the range of ssDNA:PtNP ratios examined, a rapid decrease in the collision amplitude is found over the same (increasing) range of ssDNA surface coverages (Figure 3f). The amplitude decreases from 49 ± 24 pA for naked PtNPs to 8 ± 2 pA for both the 50:1 ssDNA:PtNP ratios of the 5-mer and 25-mer. As discussed in the Supporting Information, the decrease in current is due to the presence of DNA on the PtNPs and not to adsorption of adventitious ssDNA onto the electrode surface (arising from insufficient washing of the ssDNA/PtNPs). Note that MPOH-modified PtNPs exhibit much less change in collision current amplitude and frequency than the ssDNA/PtNPs (Figure S5).

From the data discussed thus far, we conclude that the decrease in current amplitude and collision frequency for the ssDNA- and MPOH-modified PtNPs arises from blockage of the catalytic sites on the PtNPs by the thiol groups. Additionally, but probably less important, the presence of ssDNA prevents intimate contact between the PtNPs and the electrode surface, and hence reduces the likelihood of electron transfer.

Collisions between ssDNA- or MPOH-Modified PtNPs and Naked Hg UMEs. Figure 4 presents results analogous to those discussed in the previous section, but for surface-modified PtNPs at Hg, rather than Au, UMEs. For example, 4a shows $i-t$ curves comparing collisions of 10 pM naked PtNPs to collisions between 10 pM 5-mer/PtNP conjugates for ratios between 5:1 and 50:1 (recall these are the ratios of ssDNA:PtNPs in the solution used to modify the PtNPs, not the actual surface concentrations). Similar $i-t$ plots, comparing collisions of naked PtNPs and 25-mer/PtNP and MPOH/PtNP conjugates at naked Hg UMEs are provided in Figures S4 and S5. As shown in Figure

DOI: 10.1021/acs.langmuir.5b03639

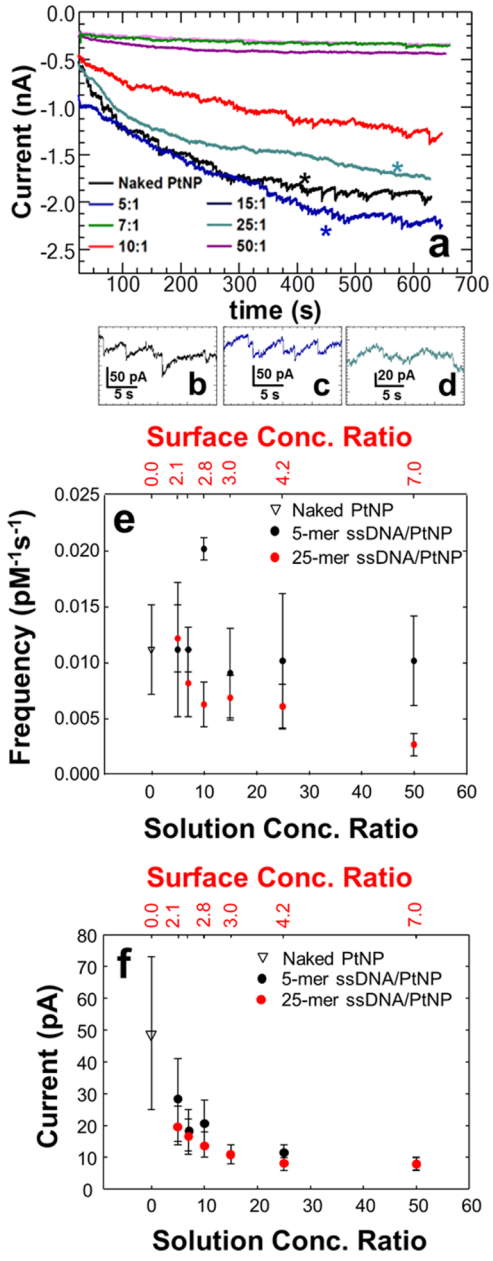

Figure 3. Collision data obtained using naked Au UMEs. (a) Chronoamperometric data obtained using naked and 5-mer-modified PtNPs. The 5-mer:PtNP ratios shown in the legend (5:1 to 50:1) reflect the solution concentrations used for modification, not the actual surface concentrations of ssDNA. (b–d) Expanded views of the data in (a) in the regions marked with an asterisk for the (b) naked, (c) 5:1, and (d) 25:1 5-mer:PtNP ratios. Plots of (e) collision frequency and (f) transient currents as a function of both the 5-mer:PtNP solution ratio (lower horizontal axes) and the actual surface coverage of the 25-mer on the PtNPs (upper horizontal axes). The chronoamperometric data from which plots (e) and (f) originated were obtained using 10 pM PtNPs, and the duration of each experiment was ~600 s. Error bars represent the standard deviation of measured transients collected from three independent experiments. The legend in (a) applies to the plots in (b–d).

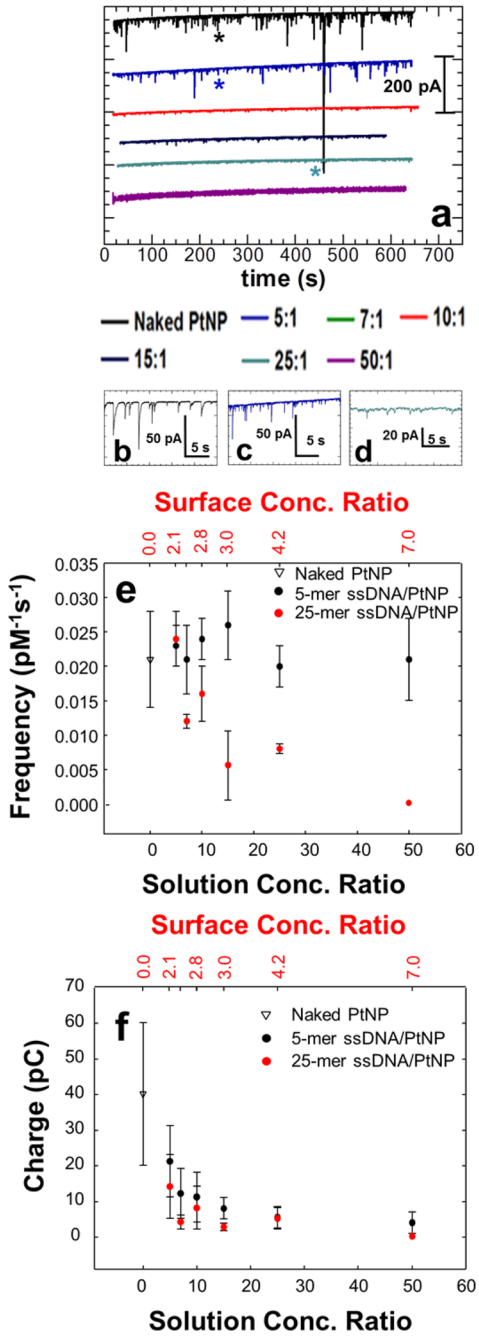

Figure 4. Collision data obtained using naked Hg UMEs. (a) Chronoamperometric data obtained using naked and 5-mer-modified PtNPs. The 5-mer:PtNP ratios shown in the legend (5:1 to 50:1) reflect the solution concentrations used for modification, not the actual surface concentrations of ssDNA. (b–d) Expanded view of the data in (a) in the regions marked with an asterisk (b) naked, (c) 5:1, and (d) 25:1 5-mer:PtNP ratios. Plots of (e) collision frequency and (f) transient charge as a function of both the 5-mer:PtNP solution ratio (lower horizontal axes) and the actual surface coverage of the 25-mer on the PtNPs (upper horizontal axes). The chronoamperometric data from which plots (e) and (f) originate were obtained using 10 pM PtNPs, and the duration of each experiment was ~600 s. Error bars represent the standard deviation of measured transients collected from three independent experiments. The legend below (a) applies to plots (a–d).

4a–d, the *i*–*t* plots display the characteristic spike-shaped current transients common for Hg UMEs.[8−10]

The results for naked Hg electrodes are shown in Figure 4a–d, and they exhibit the same trends observed for naked Au electrodes (Figure 3a–d). That is, as the concentration of 5-mer on the PtNP surface increases, the charge decreases. For example, the average charge is 40 ± 17 pC for naked PtNPs colliding with a naked Hg UME, but after modifying the PtNPs with a 5:1 ratio of

5-mer ssDNA:PtNPs the average charge decreases to 21 ± 10 pC. No collisions are observed for the 50:1 25-mer/PtNP ratio on Hg UMEs.

Figures 4e and 4f display plots of the collision frequency and charge, respectively, for collisions involving 5-mer/PtNP and 25-mer/PtNP conjugates at naked Hg UMEs. Like Figures 3e and 3f, Figure 4e and 4f, present the frequency and charge data as a function of both the 5-mer:PtNP solution ratio (lower horizontal axis) and the measured 25-mer surface concentration (upper horizontal axis). The collision frequency remains approximately constant at ~0.021 pM^{-1} s^{-1} over the entire range for collisions of the 5-mer/PtNP and MPOH/PtNP (Figure S5) conjugates. However, the collision frequency decreases from 0.021 ± 0.005 to 0.008 ± 0.0007 pM^{-1} s^{-1} for the 25:1 25-mer/PtNP conjugates, presumably due to a change in the diffusional flux of 25-mer/PtNP conjugates.

As observed for the Au UMEs, the charge-per-collision for the Hg UMEs decreases quickly as the thiol concentration on the PtNP surface increases (Figure 4f). For example, the naked PtNPs yield an average collision charge of 40 ± 20 pC, but the charge arising from collisions with the 50:1 5-mer/PtNPs decreases to 3.8 ± 3 pC. Likewise, the charge for the highest 25-mer:PtNP ratio investigated, 25:1, decreases to 5.0 ± 3 pC.

Two final points are worth mentioning. First, there is a possibility that the decrease in collision charge and frequency could, in part, be due to adsorption of free DNA, resulting from incomplete washing or desorption from the modified PtNPs, onto the surface of the Hg UME. This seems unlikely, however, given the results of control experiments discussed in the Supporting Information. Second, as shown in Figure S5, the MPOH/PtNP conjugates exhibit a much smaller decrease in charge, compared to ssDNA, as the coverage of MPOH is increased on the PtNPs. The frequency, however, remains relatively unchanged throughout the range of MPOH:PtNP ratios evaluated.

SUMMARY AND CONCLUSIONS

Our motivation for developing a better understanding of collisions at DNA-coated surfaces derives from our long-term interest in using ECA to detect biological targets. DNA sensing is of special interest in this regard, but that will require a means for integrating DNA into collision experiments. An obvious strategy for DNA sensing built on the ECA approach could involve a sandwich assay in which the target links a catalytic DNA-modified NP to a DNA-modified electrode surface via hybridization. One then has to ask how the presence of ssDNA on these surfaces affects ECA. That is the question we sought to answer here.

To address this question, we examined the effect of short (5-mer) and long (25-mer) thiolated DNA on the magnitude and frequency of ECA signals. The results are quite clear. When ssDNA is present on an Au or Hg electrode at low surface concentration, it has little impact on the signal magnitude or frequency of ECA collisions with naked PtNPs. Moreover, the background $i-t$ response is smaller and more stable than at nominally naked Au UME surfaces, and this makes it easier to distinguish and measure current transients. In contrast, when DNA is immobilized on the electrocatalytic PtNPs and the electrodes are naked, more ominous trends emerge. Specifically, as the surface concentration of ssDNA on the PtNP surface increases, the magnitude and frequency of current transients decrease. This trend is most apparent for the longer 25-mer.

We interpret these results as follows. When ssDNA is immobilized at high concentration on the PtNPs, the catalytic surface sites on the NP are blocked. Because the signaling reaction, oxidation of N_2H_4, is an inner-sphere electrochemical process, it requires intimate contact between N_2H_4 and Pt. The presence of ssDNA on the PtNPs (particularly long ssDNA oligonucleotides or high surface concentrations) reduces the likelihood of this configuration being achieved. In addition, it is also possible that electrostatic interactions between the ssDNA-modified PtNPs and the charged electrode interface reduces the likelihood of collisions. In contrast, the presence of ssDNA on the electrode is not nearly as detrimental. There are two reasons for this. First, the coverages of ssDNA used in these experiments ranged from 1 to 10% of a monolayer, and hence there are presumably naked patches on the electrode surfaces available for collisions. Second, PtNPs only need to come within a few nanometers of the electrode surface to be in electrochemical equilibrium with it.[44] The experimental results reported here indicate this to be achievable.

We conclude that, for DNA detection using ECA, modification of the electrode with receptors is not a limiting consideration and, at least under the conditions used in our experiments, can actually improve quantitative detection compared to naked Au electrodes. However, it is quite clear that the number of receptors present on the PtNPs must be kept low so that a significant fraction of the surface is available for catalytic reactions. We are presently working on strategies to put these findings into practice, and the results of those studies will be reported in due course.

ASSOCIATED CONTENT

Supporting Information

The Supporting Information is available free of charge on the ACS Publications website at DOI: 10.1021/acs.langmuir.5b02620.

Sizing of PtNPs by electron microscopy; discussion of UME modification and characterization; supplemental collision data for modified and naked UMEs; UV/vis data analysis of ssDNA/PtNP conjugates; discussion of the influence of unbound ssDNA on experiments involving naked UMEs; and evaluation of the stability of ssDNA/PtNP conjugates in the presence of N_2H_4 (PDF)

AUTHOR INFORMATION

Corresponding Author

*E-mail: crooks@cm.utexas.edu. Tel: 512-475-8674.

Notes

The authors declare no competing financial interest.

ACKNOWLEDGMENTS

We gratefully acknowledge financial support from the U.S. Defense Threat Reduction Agency (Grant No. HDTRA1-11-1-0005). The Robert A. Welch Foundation (Grant F-0032) provides sustained support for our research. We also appreciate helpful discussions with Prof. Allen J. Bard (UT Austin) and Prof. Bo Zhang (University of Washington). We also thank Dr. Dwight Romanovicz (ICMB, UT Austin) for assistance with the TEM measurements.

REFERENCES

(1) Bard, A. J.; Zhou, H.; Kwon, S. J. Electrochemistry of Single Nanoparticles via Electrocatalytic Amplification. *Isr. J. Chem.* **2010**, *50*, 267−276.

(2) Wang, W.; Tao, N. Detection, Counting, and Imaging of Single Nanoparticles. *Anal. Chem.* **2014**, *86*, 2−14.

(3) Kleijn, S. E. F.; Lai, S. C. S.; Koper, M. T. M.; Unwin, P. R. Electrochemistry of Nanoparticles. *Angew. Chem., Int. Ed.* **2014**, *53*, 3558−3586.

(4) Xiao, X.; Bard, A. J. Observing Single Nanoparticle Collisions at an Ultramicroelectrode by Electrocatalytic Amplification. *J. Am. Chem. Soc.* **2007**, *129*, 9610−9612.

(5) Kwon, S. J.; Fan, F.-R. F.; Bard, A. J. Observing Iridium Oxide (IrOx) Single Nanoparticle Collisions at Ultramicroelectrodes. *J. Am. Chem. Soc.* **2010**, *132*, 13165−13167.

(6) Zhou, H.; Fan, F.-R. F.; Bard, A. J. Observation of Discrete Au Nanoparticle Collisions by Electrocatalytic Amplification Using Pt Ultramicroelectrode Surface Modification. *J. Phys. Chem. Lett.* **2010**, *1*, 2671−2674.

(7) Wakerley, D.; Guell, A. G.; Hutton, L. A.; Miller, T. S.; Bard, A. J.; Macpherson, J. V. Boron doped diamond ultramicroelectrodes: a generic platform for sensing single nanoparticle electrocatalytic collisions. *Chem. Commun.* **2013**, *49*, 5657−5659.

(8) Dasari, R.; Robinson, D. A.; Stevenson, K. J. Ultrasensitive Electroanalytical Tool for Detecting, Sizing, and Evaluating the Catalytic Activity of Platinum Nanoparticles. *J. Am. Chem. Soc.* **2013**, *135*, 570−573.

(9) Dasari, R.; Walther, B.; Robinson, D. A.; Stevenson, K. J. Influence of the Redox Indicator Reaction on Single Nanoparticle Collisions at Mercury and Bismuth Modified Pt Ultramicroelectrodes. *Langmuir* **2013**, *29*, 15100−15106.

(10) Dasari, R.; Tai, K.; Robinson, D. A.; Stevenson, K. J. Electrochemical Monitoring of Single Nanoparticle Collisions at Mercury-Modified Platinum Ultramicroelectrodes. *ACS Nano* **2014**, *8*, 4539−4546.

(11) Xiao, X.; Fan, F.-R. F.; Zhou, J.; Bard, A. J. Current Transients in Single Nanoparticle Collision Events. *J. Am. Chem. Soc.* **2008**, *130*, 16669−16677.

(12) Fernando, A.; Parajuli, S.; Alpuche-Aviles, M. A. Observation of Individual Semiconducting Nanoparticle Collisions by Stochastic Photoelectrochemical Currents. *J. Am. Chem. Soc.* **2013**, *135*, 10894−10897.

(13) Sardesai, N. P.; Andreescu, D.; Andreescu, S. Electroanalytical Evaluation of Antioxidant Activity of Cerium Oxide Nanoparticles by Nanoparticle Collisions at Microelectrodes. *J. Am. Chem. Soc.* **2013**, *135*, 16770−16773.

(14) Zhou, Y.-G.; Rees, N. V.; Compton, R. G. The Electrochemical Detection and Characterization of Silver Nanoparticles in Aqueous Solution. *Angew. Chem., Int. Ed.* **2011**, *50*, 4219−4221.

(15) Rees, N. V.; Zhou, Y.-G.; Compton, R. G. Making contact: charge transfer during particle-electrode collisions. *RSC Adv.* **2012**, *2*, 379−384.

(16) Stuart, E. J. E.; Tschulik, K.; Omanovic, D.; Cullen, J. T.; Jurkschat, K.; Crossley, A.; Compton, R. G. Electrochemical detection of commercial silver nanoparticles: identification, sizing, and detection in enviromental media. *Nanotechnology* **2013**, *24*, 444002.

(17) Ly, L. S. Y.; Batchelor-McAuley, C.; Tschulik, K.; Katelhon, E.; Compton, R. G. A Critical Evaluation of the Interpretation of Electrocatalytic Nanoimpacts. *J. Phys. Chem. C* **2014**, *118*, 17756−17763.

(18) Alligrant, T. M.; Nettleton, E. G.; Crooks, R. M. Electrochemical detection of individual DNA hybridization events. *Lab Chip* **2013**, *13*, 349−354.

(19) Alligrant, T. M.; Dasari, R.; Anderson, M. J.; Stevenson, K. J.; Crooks, R. M. Single Nanoparticle Collisions at Microfluidic Microband Electrodes: the Effect of Electrode Material and Mass Transfer. *Langmuir* **2014**, *30*, 13462−13469.

(20) Castaneda, A. D.; Alligrant, T. M.; Loussaert, J. A.; Crooks, R. M. Electrocatalytic Amplification of Nanoparticle Collisions at Electrodes Modified with Polyelectrolyte Multilayer Films. *Langmuir* **2015**, *31*, 876−885.

(21) Yoo, J. J.; Anderson, M. J.; Alligrant, T. M.; Crooks, R. M. Electrochemical Detection of Insulating Beads at Subattomolar Concentration via Magnetic Enrichment in a Microfluidic Device. *Anal. Chem.* **2014**, *86*, 4302−4307.

(22) Kleijn, S. E. F.; Lai, S. C. S.; Miller, T. S.; Yanson, A. I.; Koper, M. T. M.; Unwin, P. R. Landing and Catalytic Characterization of Individual Nanoparticles on Electrode Surfaces. *J. Am. Chem. Soc.* **2012**, *134*, 18558−18561.

(23) Kleijn, S. E. F.; Serrano Bou, B.; Yanson, A. I.; Koper, M. T. M. Influence of hydrazine-induced aggregation on the electrochemical detection of platinum nanoparticles. *Langmuir* **2013**, *29*, 2054−2064.

(24) Li, D.; Liu, J.; Barrow, C. J.; Yang, W. Protein electrochemistry using graphene-based nano-assembly: an ultrasensitive electrochemical detection of protein molecules *via* nanoparticle-electrode collisions. *Chem. Commun.* **2014**, *50*, 8197−8200.

(25) Kwon, S. J.; Zhou, H.; Fan, F.-R. F.; Vorobyev, V.; Zhang, B.; Bard, A. J. Stochastic electrochemistry with electrocatalytic nanoparticles at inert ultramicroelectrodes-theory and experiments. *Phys. Chem. Chem. Phys.* **2011**, *13*, 5394−5402.

(26) Park, J. H.; Zhou, H.; Percival, S. J.; Zhang, B.; Fan, F.-R. F.; Bard, A. J. Open Circuit (Mixed) Potential Changes Upon Contact Between Different Intert Electrodes-Size and Kinetic Effects. *Anal. Chem.* **2013**, *85*, 964−970.

(27) Park, J. H.; Thorgaard, S. N.; Zhang, B.; Bard, A. J. Single Particle Detection by Area Amplification: Single Wall Carbon Nanotube Attachment to a Nanoelectrode. *J. Am. Chem. Soc.* **2013**, *135*, 5258−5261.

(28) Guo, Z.; Percival, S. J.; Zhang, B. Chemically Resolved Transient Collision Events of Single Electrocatalytic Nanoparticles. *J. Am. Chem. Soc.* **2014**, *136*, 8879−8882.

(29) Xiao, X.; Pan, S.; Jang, J. S.; Fan, F.-R. F.; Bard, A. J. Single Nanoparticle Electrocatalysis: The Effect of Monolayers on Particle and Electrode on Electron Transfer. *J. Phys. Chem. C* **2009**, *113*, 14978−14982.

(30) Bigall, N. C.; Härtling, T.; Klose, M.; Simon, P.; Eng, L. M.; Eychmüller, A. Monodisperse Platinum Nanospheres with Adjustable Diameters from 10 to 100 nm: Synthesis and Distinct Optical Properties. *Nano Lett.* **2008**, *8*, 4588−4592.

(31) Jentys, A. Estimation of the mean size and shape of small metal particles by EXAFS. *Phys. Chem. Chem. Phys.* **1999**, *1*, 4059−4063.

(32) Gill, R.; Polsky, R.; Willner, I. Pt Nanoparticles Functionalized with Nucleic Acid Act as Catalytic Labels for the Chemiluminescent Detection of DNA and Proteins. *Small* **2006**, *2*, 1037−1041.

(33) Chow, K.-F.; Mavré, F.; Crooks, R. M. Wireless Electrochemical DNA Microarray Sensor. *J. Am. Chem. Soc.* **2008**, *130*, 7544−7545.

(34) Polsky, R.; Gill, R.; Kaganovsky, L.; Willner, I. Nucleic-Acid Functionalized Pt Nanoparticles: Catalytic Labels for the Amplified Detection of Biomolecules. *Anal. Chem.* **2006**, *78*, 2268−2271.

(35) Mauzeroll, J.; Hueske, E. A.; Bard, A. J. Scanning Electrochemical Microscopy. 48. Hg/Pt Hemispherical Ultramicroelectrodes: Fabrication and Characterization. *Anal. Chem.* **2003**, *75*, 3880−3889.

(36) Wightman, R. M.; Wipf, D. O. Voltammetry at Ultramicroelectrodes. In *Electroanalytical Chemistry: A Series of Advances*; Bard, A. J., Ed.; Marcel Dekker: New York, 1988; Vol. *15*, pp 267−353.

(37) Palecek, E. From Polarography of DNA to Microanalysis with Nucleic Acid-Modified Electrodes. *Electroanalysis* **1996**, *8*, 7−14.

(38) Ostatná, V.; Palecek, E. Self-Assembled Monolayers of Thiol-End-Labeled DNA at Mercury Electrodes. *Langmuir* **2006**, *22*, 6481−6484.

(39) Calvente, J. J.; Andreu, R.; González, L.; Gil, M.-L. A.; Mozo, J. D.; Roldán, E. Formation and Reductive Desorption of Mercaptohexanol Monolayers on Mercury. *J. Phys. Chem. B* **2001**, *105*, 5477−5488.

(40) Steel, A. B.; Herne, T. M.; Tarlov, M. J. Electrochemical Quantitation of DNA Immobilized on Gold. *Anal. Chem.* **1998**, *70*, 4670−4677.

(41) Zhang, J.; Song, S.; Wang, L.; Pan, D.; Fan, C. A gold nanoparticle-based chronocoulometric DNA sensor for amplified detection of DNA. *Nat. Protoc.* **2007**, *2*, 2888−2895.

DOI: 10.1021/acs.langmuir.5b02630

(42) Bard, A. J.; Faulkner, L. R. *Electrochemical Methods: Fundamentals and Applications*, 2ed.: John Wiley and Sons: New York, 2001.
(43) Ostatná, V.; Jelen, F.; Hianik, T.; Palecek, E. Electrochemical Responses of Thiolated Oligodeoxynucleotides in Cobalt-Containing Solutions. *Electroanalysis* **2005**, *17*, 1413−1420.
(44) Chazalviel, J.-N.; Allongue, P. On the Origin of the Efficient Nanoparticle Mediated Electron Transfer Across a Self-Assembled Monolayer. *J. Am. Chem. Soc.* **2011**, *133*, 762−764.
(45) Thompson, M. A. *ArgusLab*, version 4.0.1; Planaria Software LLC: Seattle, WA, 2004.
(46) Franklin, R. E.; Gosling, R. G. Molecular Configuration in Sodium Thymonucleate. *Nature* **1953**, *171*, 740−741.

DOI: 10.1021/la5026639